Sparse regularization methods in ultrafast ultrasound imaging

Adrien Besson*‡, Rafael E. Carrillo*, Miaomiao Zhang†, Denis Friboulet†, Olivier Bernard†,
Yves Wiaux‡ and Jean-Philippe Thiran*§
*Signal Processing Laboratory (LTS5), Ecole Polytechnique Fédérale de Lausanne, Lausanne, Switzerland
†CREATIS, CNRS UMR5220, University of Lyon, INSA-Lyon, University of Lyon1, Villeurbanne, France
‡Institute of Sensors, Signals and Systems, Heriot-Watt University, Edinburgh, UK
§Department of Radiology, University Hospital Center (CHUV) and University of Lausanne (UNIL), Lausanne, Switzerland

***Abstract*—Ultrafast ultrasound (US) imaging based on plane wave (PW) insonification is a widely used modality nowadays. Two main types of approaches have been proposed for image reconstruction either based on classical delay-and-sum (DAS) or on Fourier reconstruction. Using a single PW, these methods lead to a lower image quality than DAS with multi-focused beams. In this paper we review recent beamforming approaches based on sparse regularization methods. The imaging problem, either spatial-based (DAS) or Fourier-based, is formulated as a linear inverse problem and convex optimization algorithms coupled with sparsity priors are used to solve the ill-posed problem. We describe two applications of the framework namely the sparse inversion of the beamforming problem and the compressed beamforming in which the framework is combined with compressed sensing. Based on numerical simulations and experimental studies, we show the advantage of the proposed methods in terms of image quality compared to classical methods.**

***Index Terms*—Ultrasound, plane wave imaging, sparsity, compressed sensing**

I. Introduction

In the last years, ultrafast ultrasound imaging (US) based on plane wave (PW) insonification has become a widely used modality in the US community. Indeed, while conventional beamforming methods rely on a sequential transmission of a number of focused waves equal to the number of scan lines, thus limiting the frame rate to several tens of frames per second, PW imaging only needs few insonifications to reconstruct an image, enabling to reach far higher frame rates, around thousands of frames per second, and opening a whole range of applications [1].

The ability to perform ultrafast imaging is closely linked to the possibility to implement efficient beamforming methods. Nowadays, two main approaches have been developed namely spatial-based approaches [2] where the image is reconstructed using delay-and-sum (DAS) technique, and Fourier-based approaches [3]–[5] where the Fourier spectrum of the received raw data is used to reconstruct the final image.

The use of few PW insonifications usually leads to a lower image quality than classical DAS approaches with multi-focused beams [2]. Indeed, instead of being focused to the region of interest, the energy carried by a PW is spread over all the medium which induces a decrease of the signal to noise ratio. Moreover, the information carried by a PW allows to retrieve partial information of the final image which makes the beamforming problem ill-posed. In addition, since all the beamforming methods are based on numerical approximations of continuous expressions, they implicitly make use of gridding and interpolation which lead to measurement inaccuracies and thus to a decrease of the image quality [6].

Compressed sensing (CS) is a mathematical framework to recover signals from incomplete information [7] that has been successfully applied to medical US imaging (see [8], [9] and references therein). In this paper we propose a general framework based on reformulating the beamforming process, either Fourier-based or spatial-based, as an inverse problem which is solved by exploiting sparsity of US images in a redundant dictionary. We detail two main applications of the proposed framework, only differing in the measurement model. The first one is the use of sparse regularization for image quality enhancement [8]. The second one is a compressed beamforming approach in which the desired image is retrieved from only few samples of the raw data.

The paper is organized as follows. Section II reviews the existing beamforming approaches. Section III describes the proposed framework and details a general formulation of the inverse problem. Sections IV and V illustrate the two applications of the proposed framework and show the benefits of the proposed approach through numerical simulations and *in vivo* experiments.

II. Background

After a PW insonification, the received signal $r(x_i, t)$ at the US probe (linear array of transducers), in a transducer at position x_i and at time t, the so called raw data, consists of backscattered echoes from the medium. In order to be exploited, the positions of the inhomogeneities are inferred from these echoes in the process called beamforming. The signal obtained after beamforming is usually denoted as radio frequency (RF) signal and will be designated by $s(x, z)$ in the following sections. The conventions used in the next sections are detailed in Figure 1.

This work was supported in part by the UltrasoundToGo RTD project (no. 20NA21 145911), funded by Nano-Tera.ch. This work was also performed within the framework of the LABEX PRIMES (ANR- 11-LABX-0063) of Universite de Lyon.

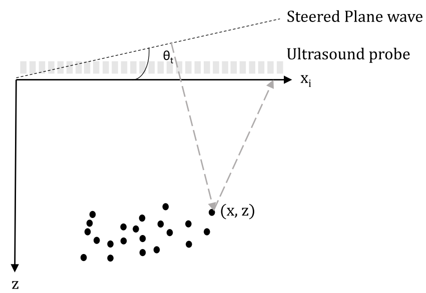

Fig. 1: Axis convention and time delay calculation for a steered PW with angle θ_t.

A. Fourier-based beamforming methods

In Fourier-based beamforming, the k-space (Fourier) representation of $s(x, z)$ is related to the k-space representation of $r(x_i, t)$ by a frequency remapping [3]. Thus, the raw data are linked to the desired image through a composition of a non-uniform Fourier transform (NUFT) which projects the desired image on the k-space of the raw data and an inverse 2D Fourier Transform (FT) [6]. Three main approaches for Fourier-based beamforming have been developed in the literature which differ in the frequency remapping. The first model developed by Lu *et al.* uses the X-waves relationship to model the behaviour of the transducer arrays at transmission and reception [10]. Formally, the following remapping is derived:

$$\left\{ \begin{array}{ll} k_x & = k'_x - k'_z \sin(\theta_t) \\ k & = \frac{k'^2_x + k'^2_z}{2k'_z \cos(\theta_t) + 2k'_x \sin(\theta_t)}, \end{array} \right. \tag{1}$$

where (k_x, k) denotes the k-space coordinates of the raw data with $k = \frac{f}{c}$ and f the temporal frequency, and (k'_x, k'_z) denotes the k-space coordinates of the desired image. The second approach, proposed by Garcia *et al.*, is based on the Stolt's migration technique and proposes the following remapping [4]:

$$\left\{ \begin{array}{ll} k_x & = k'_x \\ k & = \frac{\hat{c}}{c} sign(k'_z) \sqrt{k'^2_z + k'^2_x} \end{array} \right. \tag{2}$$

with $\hat{c} = \frac{c}{\sqrt{1+cos(\theta_t)+sin^2(\theta_t)}}$.

Very recently, Bernard *et al.* demonstrated, using Fourier slice theorem, that the temporal FT of a received PW steered with a given angle θ_t is a radial line in the k-space of the desired image [5].

B. Spatial-based beamforming method

Spatial-based approaches for beamforming relies on the so called DAS method [11] which has been applied to PW imaging by Montaldo *et al.* in [2]. In this technique, the travel-time curve corresponding to a given (x, z) is estimated and all the backscattered echoes lying on this curve are integrated. The value of this integral is then assigned to the corresponding point in the desired image. Thus, for a given PW insonification with angle θ_t, the raw data $r(x_i, t)$ can be obtained using the following relationship [12]:

$$r(x_i, t) = \iint_{(x,z)\in\Omega} s(x, z)\, dxdz, \tag{3}$$

where $\Omega = \left\{(x, z) \mid (ct - z\cos(\theta_t) - x\sin(\theta_t))^2 - (x - x_i)^2 - z^2 = 0\right\}$. If we consider a PW with normal incidence ($\theta_t = 0$), then the integral (3) can be modified into the following equation:

$$r(x_i, t) = \int_{\alpha\in\mathbb{R}} s(x(\alpha), z(\alpha)) \sqrt{1 + \frac{(\alpha - x_i)^2}{(ct)^2}} d\alpha, \tag{4}$$

with $x(\alpha) = \alpha$ and $z(\alpha) = \frac{1}{2ct}\left((ct)^2 - (\alpha - x_i)^2\right)$.

III. General framework

A. The inverse problem

Sparse regularization methods mainly rely on two pillars, namely the formulation of the considered problem as an inverse problem and the compressibility of the desired images in a given model. Formally, we firstly derive a linear measurement model $\mathsf{H} \in \mathbb{R}^{N\times M}$ such that:

$$\boldsymbol{r} = \mathsf{H}\boldsymbol{s} + \boldsymbol{n} \tag{5}$$

with $\boldsymbol{r} \in \mathbb{R}^N$ the discretized raw data, $\boldsymbol{s} \in \mathbb{R}^M$ the RF image and $\boldsymbol{n} \in \mathbb{R}^N$ the measurement noise, and we secondly provide a model $\Psi \in \mathbb{R}^{M\times P}$ such that $\boldsymbol{s}$ has a sparse decomposition $\boldsymbol{\gamma} \in \mathbb{R}^P$ on Ψ, *i.e.* such that $\boldsymbol{s} = \Psi\boldsymbol{\gamma}$ and $\boldsymbol{\gamma}$ has few non-zero elements. We retrieve $\boldsymbol{s}$ from $\boldsymbol{r}$ by solving the following convex problem (synthesis formulation):

$$\min_{\bar{\boldsymbol{s}}\in\mathbb{C}^N} \|\Psi^\dagger \bar{\boldsymbol{s}}\|_1 \text{ subject to } \|\boldsymbol{r} - \mathsf{H}\bar{\boldsymbol{s}}\|_2 \leq \epsilon, \tag{6}$$

where $\|\cdot\|_1$ denotes the ℓ_1-norm, $\Psi^\dagger$ denotes the adjoint operator of Ψ and $\bar{s}$ designates the RF image. The choice of the ℓ_1-norm is a convex relaxation to promote sparsity. While several methods may be applied to automatically identify the best value of the regularization parameter ϵ, the choice of the optimal parameters is out of the scope of the paper. In the study, ϵ is considered to be empirically tuned by the user based on visual quality.

B. The sparsifying model

In this paper, the average sparsity model proposed in [13] is used. This model has been previously studied in the context of US images in [8]. The dictionary, composed of a concatenation of several frames, enables to better capture image structures that are often sparse in several frames, thus leading to improved image reconstructions compared to single frame models.

In this study, the dictionary is composed of the concatenation of Daubechies wavelet bases from Daubechies 1 (Db1) to Daubechies 8 (Db8). Thus,

$$\Psi = \frac{1}{\sqrt{q}}[\Psi_1, ..., \Psi_\mathsf{q}]$$

where $q = 8$ and Ψ_i denotes i-th Daubechies wavelet. Db1 is the Haar basis promoting piece-wise smooth signals while Db2 to Db8 provide smoother sparse decompositions. The sparsity prior used to promote average sparsity is thus:

$$\left\|\Psi^{\dagger}\boldsymbol{s}\right\|_1 = \sum_{i=1}^{q}\left\|\Psi_{\mathrm{i}}^{\dagger}\boldsymbol{s}\right\|_1.$$

IV. Sparse regularization for image quality enhancement

A. Measurement operators

The first application of the framework described in Section III aims at enhancing the quality of the reconstruction for PW imaging. In order to derive the measurement models associated with the methods described in Section II, we firstly introduce the following gridding of the continuous image space:

$$\begin{cases} x &= \left\{(m-1)\frac{L}{N_X},\ \forall m \in \left\{-\frac{N_X}{2}+1,...,\frac{N_X}{2}\right\}\right\} \\ z &= \left\{\frac{(l-1)Z_{max}}{N_Z},\ \forall l \in \{1,...,N_Z\}\right\} \end{cases} \tag{7}$$

with L the width of the probe, N_X the number of image samples in the lateral direction, N_Z the number of image samples in the axial direction and Z_{max} the maximum depth. The gridding of the raw data is imposed by the number of transducers in the lateral direction and by the sampling frequency in the axial direction according to the following equations:

$$\begin{cases} x_i &= \left\{(m-1)p_t - \frac{N_t}{2}p_t,\ \forall m \in \{1,...,N_t\}\right\} \\ t &= \left\{\frac{(l-1)}{f_s},\ \forall l \in \{1,...,N_r\}\right\} \end{cases} \tag{8}$$

with N_r the number of raw data samples in the axial direction, f_s the sampling frequency, p_t the probe's pitch and N_t the number of transducers in the probe. We derive the two matrices $\mathsf{S} = (S_{kl})_{k\in\{1,...,N_Z\},l\in\{1,...,N_X\}}$ and $\mathsf{R} = (R_{ij})_{i\in\{1,...,N_r\},j\in\{1,...,N_t\}}$ which are respectively the discretization of s and r on the grids (7) and (8) respectively. We define $\boldsymbol{r}$ and $\boldsymbol{s}$ as vectorized versions of R and S obtained by concatenating the columns of the matrices.

1) Fourier-based model: From equation (7), the corresponding grid of the image k-space can be deduced:

$$\begin{cases} k'_x &= \left\{\frac{2\pi(m-1)}{L},\ \forall m \in \left\{\frac{-N_X}{2}+1,...,\frac{N_X}{2}\right\}\right\} \\ k'_z &= \left\{\frac{2\pi(l-1)}{Z_{max}},\ \forall l \in \{1,...,N_Z\}\right\}. \end{cases} \tag{9}$$

The same reasoning can be applied to deduce the k-space grid of the raw data (k_x, k). Given the discretized RF image $\boldsymbol{s}$, the k-space representation $\boldsymbol{y}$ of the raw data on the grid (k_x, k) is obtained by applying a composition of a 2D discrete Fourier transform (DFT) F_S on the grid (k'_x, k'_z) followed by an interpolation on (k_x, k). This operator, known as the non uniform fast Fourier transform (NUFFT) [14], can be written as GF_S in which G is a matrix implementing the convolutional interpolation kernel. Then, $\boldsymbol{r}$ is obtained from $\boldsymbol{y}$ by a 2D inverse DFT $\mathsf{F}_R^{\dagger}$ on the grid (k_x, k) and the following equation holds:

$$\boldsymbol{r} = \mathsf{F}_R^{\dagger}\mathsf{GF}_S\boldsymbol{s} + \boldsymbol{n} = \mathsf{H}_F\boldsymbol{s} + \boldsymbol{n} \tag{10}$$

with $\boldsymbol{n} \in \mathbb{R}^N$ representing the noise induced by the model inaccuracies and H_F the measurement model. It has to be noted that H_F is ill-posed since the frequency content of the raw data only allows to recover partial information in the k-space of the final image and vice-versa.

2) Spatial-based model: The spatial-based model is obtained by discretizing equation (4) using the grids described in equations (7) and (8). In order to do so, we firstly discretize the continuous variable α by introducing the following vector:

$$\begin{cases} \boldsymbol{\alpha} \in \mathbb{R}^J \\ -\frac{L}{2} \leq \alpha_1 < \alpha_2 < ... < \alpha_J \leq \frac{L}{2} \end{cases}$$

with $J \in \mathbb{N}$. We thus have:

$$R_{ij} = \sum_{k=1}^{J} s\left(x\left(\alpha_k\right), z\left(\alpha_k\right)\right) C\left(\alpha_k\right),$$

with $C\left(\alpha_k\right) = \sqrt{1 + \frac{(\alpha_k - x_i)^2}{(ct)^2}}$.

In a second step, we compute each $s\left(x\left(\alpha_k\right), z\left(\alpha_k\right)\right)$ on the grid (7) using an interpolation with kernel $\mathsf{K} = (\mathsf{K}_{ij}) \in \mathbb{R}^{N_K\times N_K}$. The following equation holds:

$$R_{ij} = \sum_{k=1}^{J} C\left(\alpha_k\right) \sum_{p=1}^{N_K} \sum_{l=1}^{N_K} \mathsf{K}_{pl}\mathsf{S}_{p_{\alpha_k}+p-\lfloor\frac{N_K}{2}\rfloor, l_{\alpha_k}+l-\lfloor\frac{N_K}{2}\rfloor} \tag{11}$$

where $\lfloor\cdot\rfloor$ denotes the floor function and $(p_{\alpha_k}, l_{\alpha_k})$ is the closest point to $\left(x\left(\alpha_k\right), z\left(\alpha_k\right)\right)$ lying on the grid. In the following, we assume that $\boldsymbol{\alpha} = x$ and that K is a linear interpolation in the axial direction and can be written as $\mathsf{K} = \begin{pmatrix}1 & 0\\ 1 & 0\end{pmatrix}$. More elaborated quadrature rules (Simpson, Gauss-Legendre) and interpolation kernels may be used in (11) which should lead to better image quality. Following equation (11), R and S are related by a $4D-$matrix $\mathcal{H}_S = \left(\mathsf{H}_{\mathsf{S}_{\mathsf{ijkl}}}\right)$. $\mathcal{H}_S$ is then reduced to a 2D matrix by vectorizing both S and R and the following inverse problem is obtained:

$$\boldsymbol{r} = \mathsf{H}_S\boldsymbol{s} + \boldsymbol{n}. \tag{12}$$

As for Fourier-based beamforming, it should be noticed that H_S is ill-posed since the raw data carry only partial information on the desired image and vice-versa. In equations (10) and (12), $\boldsymbol{s}$ is retrieved from $\boldsymbol{r}$ by solving problem (6).

B. Experiments

The discretization of the continuous NUFT in Fourier-based beamforming induces measurement inaccuracies and leads to a decrease of the image quality (contrast) [8]. The usual way to address this problem is by performing a zero-padding in the k-space of the echoes which improves the accuracy of the interpolation performed in the NUFT [6]. However, such method induces a non-negligible increase of the computational complexity and the gain in terms of image quality remains limited. Moreover, the measurement operator being ill-posed due to the partial information carried in the k-space of the raw data, the adjoint of H_F does not lead to the optimal reconstruction. For spatial-based method, the quality of the reconstruction is directly linked to the pitch and sampling frequency of the probe. As for Fourier-based approach, since the raw data only contain partial information (not for all the points lying in Ω), the operator H_S is ill-posed. In order to achieve reasonable image reconstruction, the axial direction is usually sampled at far higher frequency than Nyquist frequency leading to both an higher data rate and a bigger amount of delays to be calculated [15] .

In order to show the benefits of the proposed method in terms of image quality, a numerical study of the contrast is performed. A standard linear probe whose settings are given in Table I is implemented using Field II [16], [17]. Constant speed of sound is assumed (1540 m.s^{-1}).

Parameter	Value
Number of elements (N_t)	128
Center frequency (f_0)	$5MHz$
Wavelength (λ)	0.31 mm
Sampling frequency (f_s)	$25MHz$
Pitch	0.1953 mm
Kerf	0.05 mm

TABLE I: Probe characteristics.

An anechoic cyst which is composed of a 8-mm diameter anechoic occlusion at 4 cm depth embedded in a medium with high density of scatterers (20 per resolution cell) is insonified with one PW with normal incidence. No apodization is used neither at transmission nor at reception. The RF image is reconstructed with both the classical methods described in Section II and the proposed framework. The envelope image is extracted from the reconstructed RF image, gamma-compressed using $\gamma = 0.3$ and finally converted to 8-bit gray scale to get the B-mode image. The contrast metric defined in the following equation is computed on the B-mode image [18]:

$$CR = 20 \log_{10} \frac{|\mu_t - \mu_b|}{\sqrt{\frac{\sigma_t^2 + \sigma_b^2}{2}}} \tag{13}$$

where μ_t and μ_b (σ_t^2, σ_b^2) are the means (variances) of respectively the target and the background. Table II displays the contrast values of the classical method without upsampling (column 1), with upsampling (column 2) and of the proposed framework without upsampling (column 3). The upsampling consists in a zero-padding of a factor 2 in the axial direction and a factor 1.5 in the lateral direction for the Fourier-based methods and an upsampling of a factor 4 compared to the Nyquist frequency for the spatial-based approach. While the benefit of the zero-padding on the Fourier-based approaches has already been demonstrated [6] and is visible in Table II, the increase of the sampling frequency is not so beneficial for the spatial-based approach. Indeed, a higher sampling frequency leads to a better estimation of the delays. However, since an interpolation is already performed to improve the estimation of the delays, such a high sampling frequency is not required. The results show an increase of the contrast for the proposed framework, for both Fourier-based and spatial-based approaches. Since the contrast is measured in the anechoic area, it is directly linked to the amount of noise in the reconstructed image and since the images are obtained through simulation, the only source of noise is induced by the measurement model (gridding). This decrease can be observed in the anechoic area of the B-mode images displayed on Figure 2.

	Classic	Classic upsampled	Sparse
Fourier-based approach	5.59	7.29	9.62
Spatial-based approach	7.04	7.48	9.10

TABLE II: Contrast values (in dB) for the classical methods and the sparse regularization framework. The Fourier-based approach used in the study is the Lu method [3].

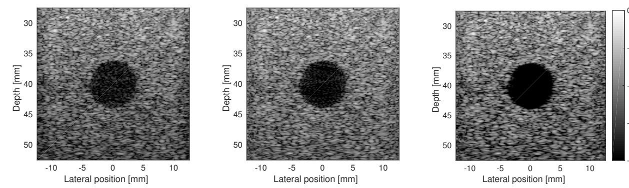

(a) Lu (b) Lu upsampled (c) Lu sparse

Fig. 2: B-mode image of the anechoic phantom obtained with 1 PW insonification and reconstructed with (a) classical Lu method (CR = 5.58 dB), (b) classical Lu method with upsampling (CR = 7.29 dB) and (c) Lu method with the proposed framework (CR = 9.62 dB) without upsampling.

V. Compressed beamforming

A. Measurement operator

The models described in equations (10) and (12) are suitable to CS-based methods since they are formulated as inverse problems. Formally, we consider an undersampled measurement vector $\boldsymbol{r_u} \in \mathbb{R}^P$ with $P \ll N$ and the corresponding projection operator $\mathsf{P} \in \mathbb{R}^{P \times N}$ such that, $p_{ij} \in \{0,1\}$, $\forall (i,j) \in \{1,...,P\} \times \{1,...,N\}$ and $\boldsymbol{r_u} = \mathsf{P}\boldsymbol{r}$. Retrieving $\boldsymbol{s}$ given $\boldsymbol{r_u}$ poses the inverse problem defined in the following equation:

$$\boldsymbol{r_u} = \mathsf{P}\left(\mathsf{H}\boldsymbol{s} + \boldsymbol{n}\right) = \mathsf{H_p}\boldsymbol{s} + \boldsymbol{n_u} \ , \tag{14}$$

with $\mathsf{H_p} = \mathsf{PH} \in \mathbb{R}^{P \times N}$, $\boldsymbol{n_u} = \mathsf{P}\boldsymbol{n}$ and H is either H_S or H_F depending on the chosen approach. $\boldsymbol{s}$ is retrieved from $\boldsymbol{r_u}$ by solving problem (6).

It can be noticed that problem (14) is close to the one described in [12] with the difference that the inverse scattering problem (not the beamforming) is formulated using Green's functions in the above mentioned paper.

B. Experiments

In the following section, the undersampling operator P is designed by randomly selecting N_c transducers at reception, with $N_c < N_t$. This non-uniform spacing has proven to be suited for CS in radar imaging [19].

The proposed method is evaluated on *in vivo* carotid images acquired with a Verasonics ultrasound scanner (Redmond, WA, USA) with a L12-5-50mm Verasonics linear probe whose settings are given on Table I. The carotid is insonified with one PW with normal incidence. No apodization is used neither in transmit nor in receive. The raw data are undersampled according to the scheme defined above and the RF image is reconstructed using the different methods. The envelope image is extracted from the reconstructed RF image, gamma-compressed using $\gamma = 0.3$ and finally converted to 8-bit gray scale to get the B-mode image. The quality of the reconstruction is evaluated by the structural similarity index (SSIM) [20] and the normalized root mean square error (NRMSE) computed on the normalized envelope image [15]. The reference images are chosen as the one obtained with the classical method with full data. Table III displays the results. As expected the higher the number of transducers, the better the quality of the reconstruction. It can also be noticed that the quality of the reconstruction is comparable between both approaches. It seems that it is slightly better with the Fourier-based method. However, this increase is not visible on the B-mode images, displayed on Figure 3. Both speckle patterns, necessary for tracking tools, as well as thickness of the carotid artery plaque are well preserved with the proposed framework.

SSIM	30	64	90
Fourier-based approach	0.78	0.86	0.92
Spatial-based approach	0.70	0.78	0.82

(a) SSIM

NRMSE	30	64	90
Fourier-based approach	0.27	0.49	0.69
Spatial-based approach	0.25	0.43	0.55

(b) NRMSE

TABLE III: (a) SSIM and (b) NRMSE values for the carotid images acquired with 30, 64 and 90 transducers (among 128) randomly chosen across the aperture.

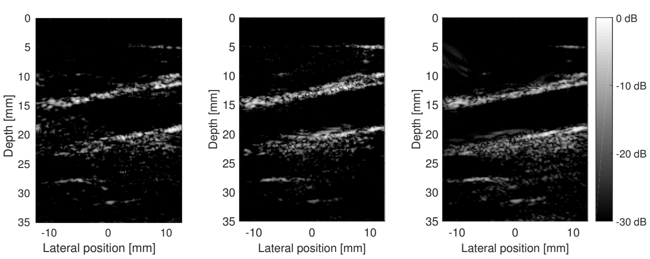

(a) (b) (c)

Fig. 3: B-mode image of the carotid obtained with 1 PW insonification and (a) 38 transducers and CS with Lu method, (b) 38 transducers and CS with spatial-based method and (c) 128 transducers and classic spatial-based approach.

VI. Conclusion

In this paper, we propose a beamforming framework for US imaging. In this framework, the beamforming process is expressed as an inverse problem and solved using a sparsity prior in a redundant dictionary. Two main applications follow on from this formulation. First it enables to increase the image quality by removing measurement artifacts induced by the gridding operation. Secondly, it is suitable to the CS framework and enables the reconstruction of high quality images from undersampled raw data acquired using only a few transducers. By alleviating data rates for acquisition, it opens the door to a whole range of applications and especially to 3D imaging where the amount of data to process remains a major limitation nowadays.

References

[1] M. Tanter and M. Fink, “Ultrafast imaging in biomedical ultrasound,” *IEEE Trans. Ultrason. Ferroelectr. Freq. Control*, vol. 61, no. 1, pp. 102–119, 2014.

[2] G. Montaldo, M. Tanter, J. Bercoff, N. Benech, and M. Fink, “Coherent plane-wave compounding for very high frame rate ultrasonography and transient elastography,” *IEEE Trans. Ultrason. Ferroelectr. Freq. Control*, vol. 56, no. 3, pp. 489–506, 2009.

[3] J. Y. Lu and J. F. Greenleaf, “Ultrasonic nondiffracting transducer for medical imaging,” *IEEE Trans. Ultrason. Ferroelectr. Freq. Control*, vol. 37, no. 5, pp. 438–447, 1990.

[4] D. Garcia, L. Le Tarnec, S. Muth, E. Montagnon, J. Poree, and G. Cloutier, “Stolt’s f-k migration for plane wave ultrasound imaging,” *IEEE Trans. Ultrason. Ferroelectr. Freq. Control*, vol. 60, no. 9, pp. 1853–1867, 2013.

[5] O. Bernard, M. Zhang, F. Varray, P. Gueth, J.-P. Thiran, H. Liebgott, and D. Friboulet, “Ultrasound Fourier slice imaging: a novel approach for ultrafast imaging technique,” in *2014 IEEE Int. Ultrason. Symp.*, 2014.

[6] P. Kruizinga, F. Mastik, N. de Jong, A. F. W. van der Steen, and G. van Soest, “Plane-wave ultrasound beamforming using a nonuniform fast Fourier transform.,” *IEEE Trans. Ultrason. Ferroelectr. Freq. Control*, vol. 59, no. 12, pp. 2684–91, 2012.

[7] E. J. Candes, “Compressive sampling,” in *Proc. Int. Congr. Math.* Madrid, Spain, 2006.

[8] R. E. Carrillo, A. Besson, M. Zhang, D. Friboulet, Y. Wiaux, J.-P. Thiran, and O. Bernard, “A sparse regularization approach for ultrafast ultrasound imaging,” in *IEEE Int. Ultrason. Symp.*, 2015.

[9] H. Liebgott, A. Basarab, D. Kouame, O. Bernard, and D. Friboulet, “Compressive sensing in medical ultrasound,” in *2012 IEEE Int. Ultrason. Symp.*, 2012.

[10] J. Y. Lu and J. F. Greenleaf, “Pulse-echo imaging using a nondiffracting beam transducer.,” *Ultrasound Med. Biol.*, vol. 17, no. 3, pp. 265–81, 1991.

[11] T.L. Szabo, *Diagnostic Ultrasound Imaging: Inside Out*, Academic Press series in biomedical engineering. Elsevier Academic Press, 2004.

[12] G. David, J.-L. Robert, B. Zhang, and A. F. Laine, “Time domain compressive beam forming of ultrasound signals,” *J. Acoust. Soc. Am.*, vol. 137, pp. 2773–2784, 2015.

[13] R. E. Carrillo, J. D. McEwen, D. Van De Ville, J.-P. Thiran, and Y. Wiaux, “Sparsity averaging for compressive imaging,” *IEEE Signal Process. Lett.*, vol. 20, no. 6, pp. 591–594, 2013.

[14] J. A. Fessler and B. P. Sutton, “Nonuniform fast fourier transforms using min-max interpolation,” *IEEE Trans. Signal Process.*, vol. 51, no. 2, pp. 560–574, 2003.

[15] T. Chernyakova and Y. C. Eldar, “Fourier-domain beamforming: The path to compressed ultrasound imaging,” *IEEE Trans. Ultrason. Ferroelectr. Freq. Control*, vol. 61, no. 8, pp. 1252–1267, 2014.

[16] J. A. Jensen and N. B. Svendsen, “Calculation of pressure fields from arbitrarily shaped, apodized, and excited ultrasound transducers,” *IEEE Trans. Ultrason. Ferroelectr. Freq. Control*, vol. 39, no. 2, pp. 262–267, 1992.

[17] J. A. Jensen, “FIELD: A Program for Simulating Ultrasound Systems,” in 10^{th} *nordicbaltic conference on biomedical imaging*, 1996.

[18] M. C. Van Wijk and J. M. Thijssen, “Performance testing of medical ultrasound equipment: Fundamental vs. harmonic mode,” *Ultrasonics*, vol. 40, pp. 585–591, 2002.

[19] L. C. Potter, E. Ertin, J. T. Parker, and M. Cetin, “Sparsity and Compressed Sensing in Radar Imaging,” *Proc. IEEE*, vol. 98, no. 6, pp. 1006–1020, 2010.

[20] Z. Wang, A. C. Bovik, H. R. Sheikh, and E. P. Simoncelli, “Image Quality Assessment: From Error Visibility to Structural Similarity,” *IEEE Trans. Image Process.*, vol. 13, no. 4, pp. 600–612, 2004.